Simulation of systematic site amplification effects observed at Heathcote Valley during the 2010-2011 Canterbury earthquake sequence

S. Jeong & B.A. Bradley

Department of Civil and Natural Resources Engineering, University of Canterbury, Christchurch

2015 NZSEE Conference

ABSTRACT: The strong motion station at Heathcote Valley School (HVSC) recorded unusually high peak ground accelerations (2.21g vertical and 1.41g horizontal) during the February 2011 Christchurch earthquake. Ground motions recorded at HVSC in numerous other events also exhibited consistently higher intensities compared with nearby strong motion stations. We investigated the underlying causes of such high intensity ground motions at HVSC by means of 2D dynamic finite element analyses, using recorded ground motions during the 2010-2011 Canterbury earthquake sequence. The model takes advantage of a LiDAR-based digital elevation model (DEM) to account for the surface topography, while the geometry and dynamic properties of the surficial soils are characterized by seismic cone penetration tests (sCPT) and Multi-Channel Analyses of Surface Waves (MASW). Comparisons of simulated and recorded ground motions suggests that our model performs well for distant events, while for near-field events, ground motions recorded at the adopted reference station at Lyttelton Port are not reasonable input motions for the simulation. The simulations suggest that Rayleigh waves generated at the inclined interface of the surficial colluvium and underlying volcanic rock strongly affect the ground motions recorded at HVSC, in particular, being the dominant contributor to the recorded vertical motions.

1 INTRODUCTION

Numerous intense ground motions were recorded during the 22 February 2011 Christchurch earthquake. Peak ground acceleration recorded at Heathcote Valley School station (HVSC) exceeded 2g in vertical component, and 1.4g in horizontal component (Bradley and Cubrinovski 2011). Other ground motions recorded at HVSC during the 2010-2011 Canterbury earthquake sequence also exhibited consistently higher intensities compared with nearby strong motion stations (Bradley 2012; Bradley 2013) . Figure 1 shows a side-by-side comparison of ground motions recorded at Heathcote Valley School station (HVSC) and the nearby Lyttelton Port Company station (LPCC), in which the motions at HVSC exhibit much higher amplitudes. The locations of these two stations are shown in Figure 2.

HVSC is located close to the edge of Heathcote valley, where shallow, firm colluvium sediments mantle weathered volcanic rock. Heathcote valley is a v-shaped valley facing north, surrounded by the volcanic Port Hills. Fine silts (loess)—originated from glacial and river erosion of the Southern Alps during the cold cycles of the Quaternary—are predominant in surficial soils in the Port Hills area, which were deposited by Aeolian process and then washed down to the valley along with volcanic rock debris to form the colluvium (Brown et al. 1992). The thickness of surficial soil varies from a few meters on the ridges to 20-30 meters in the valleys.

In this paper, we present a case study of site amplification effects observed at Heathcote valley. We first present a summary of the geophysical site characterization, in which the stratigraphy and shear wave velocity of the surficial soils are estimated by synthesizing data from Seismic CPT (sCPT) downhole tests and MASW. We then performed a series of 2D site response analyses, to investigate the effects of the valley stratigraphy, the surface topography and the soil-bedrock impedance contrast, on the intensity of ground shaking at HVSC.

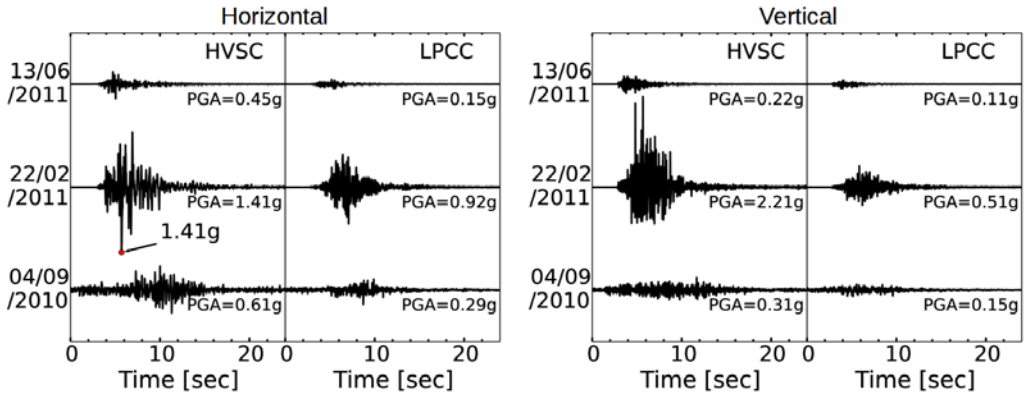

Figure 1. Comparison of acceleration time histories recorded at HVSC and LPCC (all acceleration amplitudes to scale). These stations are only 3 km apart, but exhibit a big difference in the intensities of recorded ground motions.

2 SITE CHARACTERIZATION

15 sCPT soundings and 5 MASW surveys were performed at Heathcote valley, the locations of which are plotted in Figure 2. The penetration was continued until refusal during the sCPT survey, at which point the tip resistance (q_c) usually exceeded 40 MPa, indicative of volcanic rock. sCPT surveys also accompanied the downhole tests to obtain the shear wave velocity of soils. Figure 3a summarizes the results of sCPT downhole tests, and also shows a simplified velocity profile at HVSC which was used in the numerical model. sCPT results suggest that the velocity of soils in this area strongly depends on the depth, a typical characteristic of non-plastic granular materials. This depth dependence can be approximated by a power law equation as shown in Figure 3a:

$$V_S = 144\, z^{0.39} \tag{1}$$

Seismic refraction and MASW surveys (Park et al. 1999) were performed using 24 horizontal and 24 vertical geophones and a 5 kg sledge hammer. Rayleigh and Love wave dispersion curves were obtained from the experimental data using a frequency domain beamforming technique (Johnson and Dudgeon 1992), and Geopsy (Wathelet 2005) was used for multi-modal inversion of the dispersion curves to obtain velocity profiles. The thickness of sediments obtained from CPT refusal depths, corroborated by MASW test result is spatially interpolated using the ordinary Kriging algorithm (Matheron 1963) to estimate the depth of the weathered rock, which underlies the surficial sediments. Figure 3b shows a contour plot of sediment depth. Subaxes on top and on the left of the main plot show cross sections of the valley with filled contours of shear wave velocity, approximated by Equation 1.

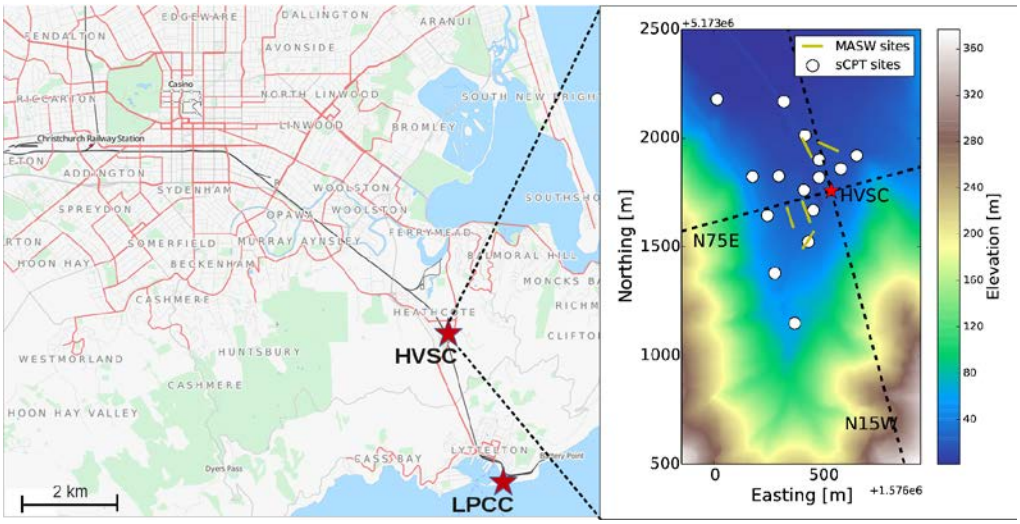

Figure 2. Location and the topography of Heathcote valley, strong motion stations HVSC and LPCC, and test sites.

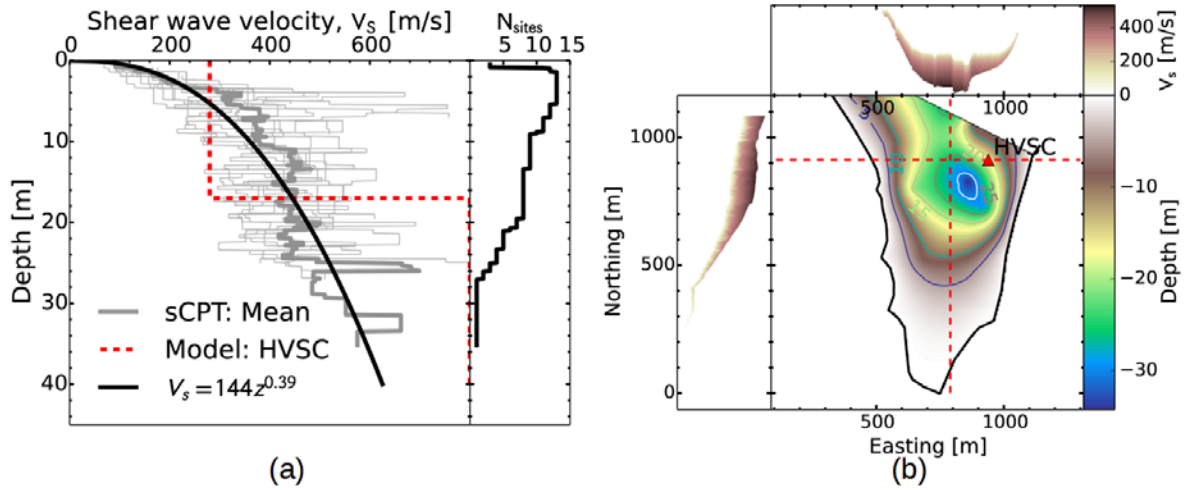

Figure 3. (a) Shear wave velocity of the loess colluvium at 15 locations in Heathcote valley as function of depth; (b) a contour plot of sediment depth obtained by spatial interpolation of sCPT and MASW data. Subaxes on top and on the left of the main plot show valley cross sections along the red dashed lines, with contours of shear wave velocity approximated by Equation 1.

3 MODEL DESCRIPTION

A series of finite element analyses were performed using OpenSees (Mazzoni et al. 2007) for 2D cross sections of the valley along 2 different azimuths: N75E (across the valley) and N15W (down the valley), as shown in Figure 2. Figure 4 shows the schematics of the mesh geometry and boundary conditions in the numerical models. Lateral boundaries are treated with the free-field boundary conditions to minimize spurious reflections. The absorbing boundary at the bottom of the models is achieved via Lysmer dashpots (Kuhlemeyer and Lysmer 1973) which are expressed by Equation 2:

$$C_X = \rho V_S, \text{ and } C_Y = \rho V_P \quad (2)$$

where ρ is the mass density; V_S and V_P are the shear and compressional velocities; and C_X and C_Y are the horizontal and the vertical dashpot coefficients. Both the soil and the rock are modelled with linear-elastic Poisson solids, with mass densities: ρ_{Soil} = 1.8 Mg/m^3 for the soil and ρ_{Rock} = 2.4 Mg/m^3 for the rock. A stiffness proportional damping is assumed with the critical damping ratio, ζ = 0.06 at the frequency, f = 16 Hz. The shear wave velocity of the soil is assumed to be a constant value of V_S = 280 m/s, which is the average shear wave velocity of the soils at HVSC based on Equation 1. This simplified velocity profile is plotted with a red dashed line in Figure 3a. The shear wave velocity of the rock is estimated from the result of MASW as V_S = 800 m/s.

The model is subjected to 9 events recorded during the 2010-2011 Canterbury earthquake sequence. Table 1 summarizes the events used for analyses, recorded at HVSC and LPCC. All input motions are filtered with a passband, f = 0.05-50 Hz. We deconvolved the acceleration time histories recorded at LPCC from the 1D linear elastic site response using the shear wave velocity profile by Wood et al. (2011), and used them as input motions prescribed at the base of model as equivalent nodal forces.

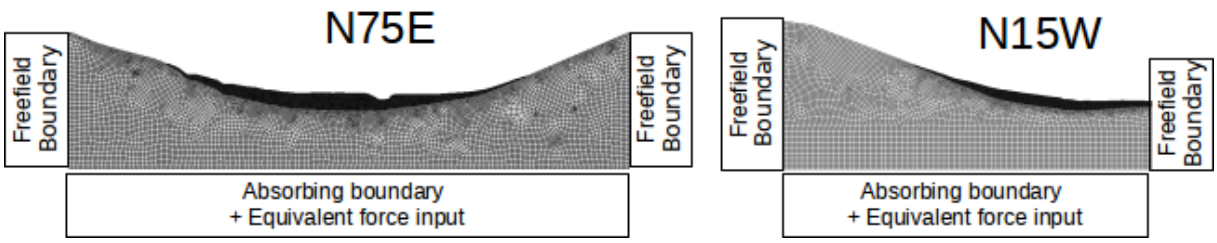

Figure 4. 2 dimensional mesh geometries and boundary conditions across the valley (left) and down the valley (right).

Table 1. Earthquake events used in the analyses, in chronological order.

Event date	M_W	HVSC			LPCC		
		R_{rup}* (km)	PGA** (g)	PGV** (cm/s)	R_{rup}* (km)	PGA** (g)	PGV** (cm/s)
04/09/2010	7.1	20.8	0.61	28.8	22.4	0.29	19.1
19/10/2010	4.8	12.8	0.09	3.2	13.1	0.02	0.71
26/12/2010	4.7	4.7	0.11	2.91	7.7	0.02	0.65
22/02/2011	6.2	3.9	1.41	81.36	7	0.92	45.59
16/04/2011	5.0	7.3	0.68	31.84	5.2	0.29	8.45
13/06/2011 (a)	5.3	4.7	0.45	13.48	5.3	0.15	5.39
13/06/2011 (b)	6.0	3.6	0.91	55.32	5.8	0.64	32.59
21/06/2011	5.2	14.9	0.26	7.95	15.6	0.07	2.11
23/12/2011	5.9	9.7	0.26	41.51	12.4	0.44	22.82

*The shortest distance from the site to the rupture surface based on Beavan et al. (2012)

**Horizontal components

4 COMPARISON WITH RECORDED GROUND MOTIONS

The two valley cross sections shows qualitatively similar responses, and in this paper, only the results of N75E cross section are presented. Figure 5 shows a comparison of simulated and recorded horizontal acceleration time series and Fourier spectra at HVSC, for the 04/09/2010 event. An excellent agreement can be observed in both time and frequency domain for this event, although this was not the universal conclusion across all events. Comparisons were much worse for some events, and it turned out that, in general, distant events showed better model performance. Figure 6 shows the comparison of simulated vs recorded response spectra at HVSC for events at 04/09/2010 and 19/10/2010, both of which have the rupture distance, R_{rup} > 10 km. 3 events with R_{rup} > 10 km produced ground motions that compare very well with recorded motions, not just in the response spectra but also in time series and Fourier spectra (not shown here for brevity).

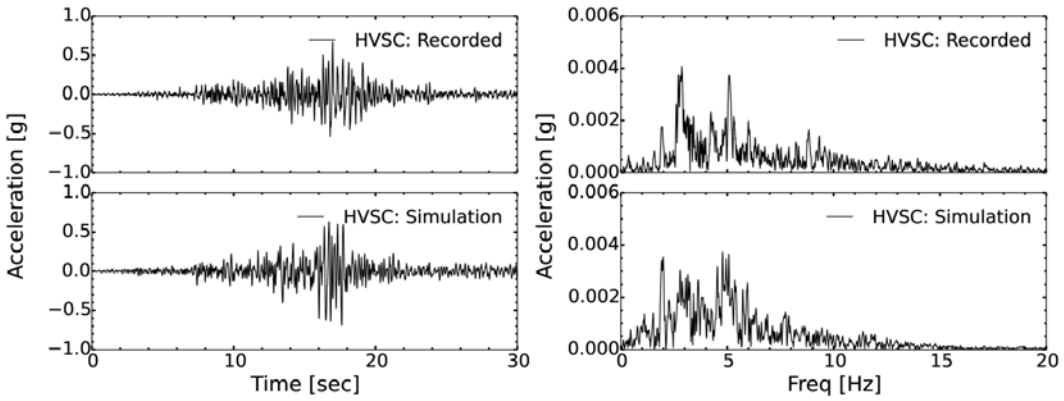

Figure 5. Comparison of simulated and recorded acceleration time histories and Fourier spectra of N75E component at HVSC, subjected to the 04/09/2010 event.

The numerical model in this study assumes linear elastic materials and vertically incident waves, using the ground motions recorded at LPCC as the input motions. Obviously, if the earthquake source is too close and the magnitude is sufficiently large, non-linear response of soils invalidates this assumption (as well as linearity assumed in the LPCC deconvolution). Also, if the actual motion at the base of Heathcote valley is much different than the motion at LPCC due to the path effects and/or if the actual incident angle from vertical is much larger than zero, it will directly impact the result of simulations

and thus make the model difficult to validate. Stations HVSC and LPCC are about 3 km apart, and considering the model assumptions it is natural to expect that the simulations may not compare very well with the records if the seismic source is too close.

One way to overcome the issue related to the path effects is to compare HVSC/LPCC spectral ratios averaged over all the considered ground motions, instead of comparing the result for individual events. LPCC is located on engineering bedrock with V_S = 1500 m/s, covered by only about 6 m of surficial soils with V_S = 300 m/s (Wood et al. 2011), which would result in negligible local site effects below 10 Hz. Therefore it is expected that actual HVSC/LPCC spectral ratio from an individual event will be mostly affected by the local site effects at HVSC and the difference in the path effects at the two stations. Assuming that the path effects (which depend on the location of the source with respect to the site) are random among the considered events, the contributions from path effects will be suppressed by averaging the spectral ratios over multiple events. Figure 7 shows the comparison of simulated and recorded HVSC/LPCC spectral ratio, averaged over all the considered ground motions. Before computing the spectral ratios, the Fourier spectra are smoothed by the Konno and Omachi smoothing window (Konno and Ohmachi 1998) with the bandwidth parameter, b = 40. Overall, the comparison was satisfactory, and both the simulation and the observation suggest that ground motions at HVSC are amplified over a broad range of frequencies, especially at f = 2-5Hz for horizontal components, and f = 5-10 Hz for vertical components.

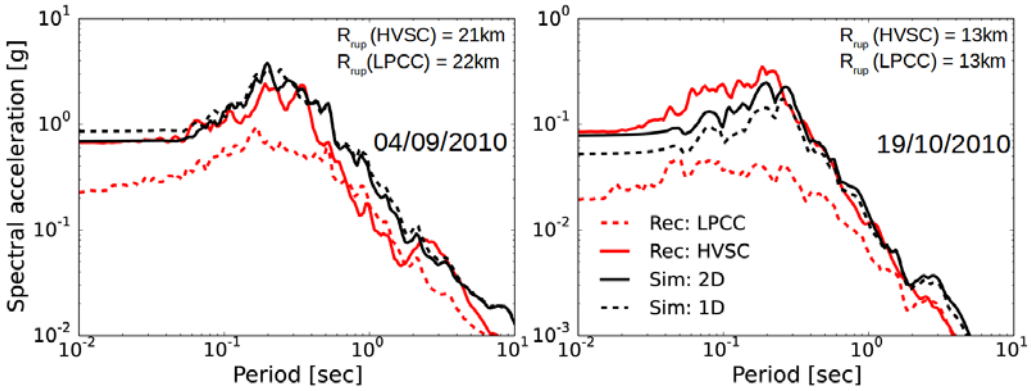

Figure 6. Comparison of simulated and recorded response spectra at HVSC for events at 04/09/2010 and 19/10/2010.

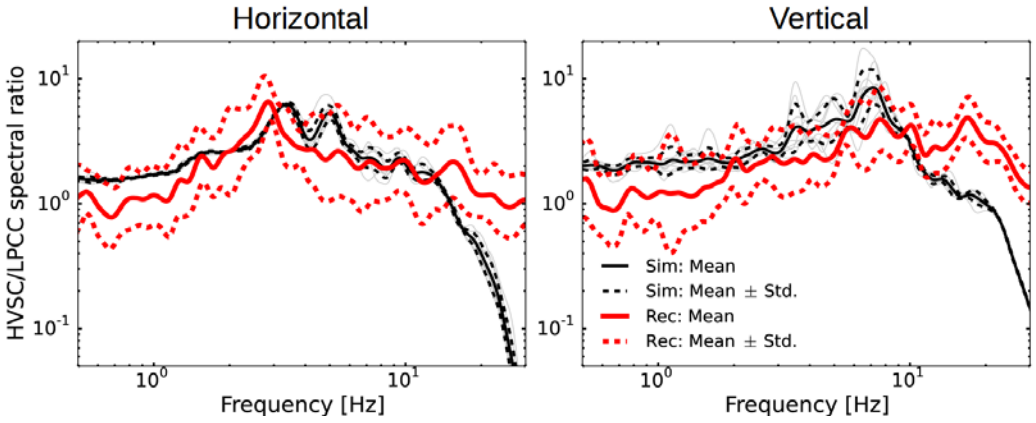

Figure 7. Simulated HVSC/LPCC spectral ratios compared with recorded spectral ratio, averaged over all considered ground motions.

5 2D SITE EFFECTS

5.1 Amplifications of the horizontal component

The amplification of ground motions can occur as a result of both the impedance contrasts between different materials and the complex stratigraphy of the basin. To help clarify the role of basin geometry in the observed amplification, Figure 8 compares the simulated 2D and 1D horizontal component transfer functions, defined as the spectral ratio of the surface response over the input motion at HVSC. The 2D response shows strong fluctuation in frequencies under 10 Hz, due to the complex wave interference caused by the reflected and mode-converted waves at the basin interface. However, the general trend of amplification function, while fluctuating rapidly, lies very close to the 1D transfer function. Considering that most recorded ground motions are broadband, the results of this (albeit simplified) analysis indicate that it is not likely that the recorded horizontal accelerations would have experienced significant amplification due to the basin geometry. This is also shown in Figure 6, which demonstrates that the response spectral accelerations from 2D and 1D responses are very close to each other, suggesting that the 1D site amplification caused by the strong impedance contrast at the soil-rock interface was likely the primary cause of strong horizontal accelerations recorded at HVSC.

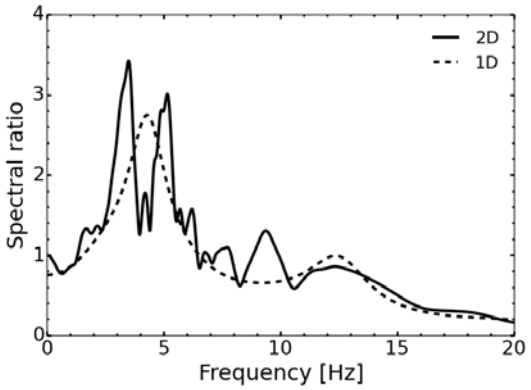

Figure 8. Comparison of 2D and 1D transfer functions at HVSC for the horizontal component, defined by the surface/input spectral ratio.

5.2 Amplifications of the vertical component

Figure 9 shows a comparison of recorded and simulated vertical acceleration time series and Fourier spectra at HVSC for the 04/09/2010 event. The simulation was performed with both the horizontal and vertical input (plotted in black solid line), and compared with the simulation with only horizontal input (red dashed line). Simulated and recorded vertical accelerations compared very well in frequencies, $f < 10$ Hz, and the comparison of results with and without the vertical input motion reveals that the mode-converted Rayleigh waves dominate the vertical response in frequencies less than 10 Hz. This finding suggests that the strong vertical motions observed at HVSC during the Canterbury earthquake sequence may be significantly affected by the mode-converted Rayleigh waves—generated near the edge of the valley due to the basin geometry and strong impedance contrast—which propagates inwards along the valley surface. A similar result was found in the comparison of vertical component response spectra shown in Figure 10, which shows that the spectral accelerations computed with and without the vertical input motion are very close to each other in periods between 0.1 and 0.3 seconds.

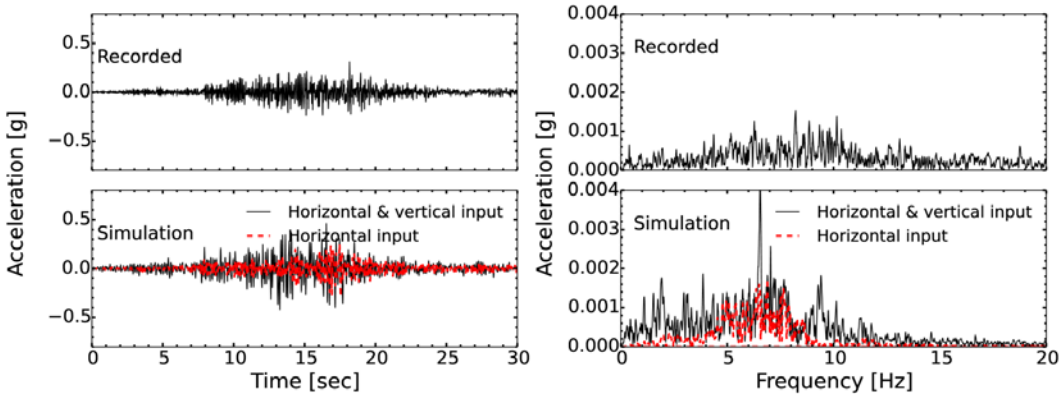

Figure 9. Vertical acceleration time history and Fourier spectra recorded at HVSC during the 04/09/2010 event, compared with the simulations: black solid line shows the result with both horizontal and vertical input motion, whereas the red dashed line used horizontal input only. Vertical accelerations at HVSC are strongly influenced by mode-converted Rayleigh waves at 5-10 Hz.

5.3 Spatial pattern of peak accelerations across the valley surface

Figure 11 illustrates the spatial pattern of simulated horizontal and vertical peak accelerations along the surface of the valley, subjected to the 04/09/2010 event. HVSC is located approximately 50 m away from an 8 m high steep slope, which was formed during the construction of Heathcote rail tunnel. The spatial pattern of PGA shows a rapid fluctuation depending on its location, a typical phenomenon in the 2D response of valleys caused by the complicated wave interference. It can be seen that the simulated PGA was maximum between HVSC and the crest of the slope, both in the horizontal and the vertical component. This observation indicates that the ground motions were also affected by the topography of the cut slope at the tunnel portal, which is known to convert the incident in-plane shear waves to Rayleigh waves (Ashford et al. 1997; Assimaki and Jeong 2013).

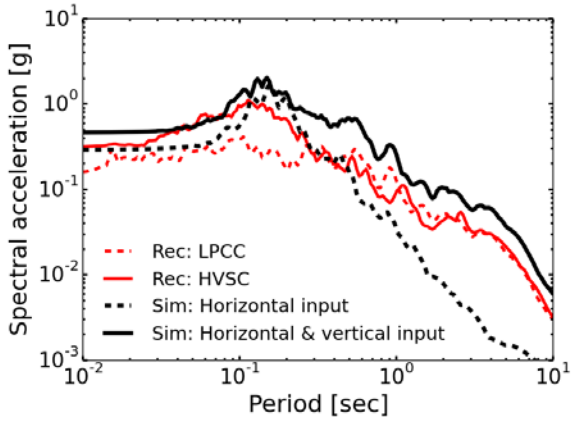

Figure 10. Vertical component response spectra at HVSC for the 04/09/2010 event. Vertical spectral acceleration using only horizontal input motion is quite close to that with both input motion in period range T = 0.1-0.3 sec, which suggests significant contribution of Rayleigh waves in the recorded vertical motions.

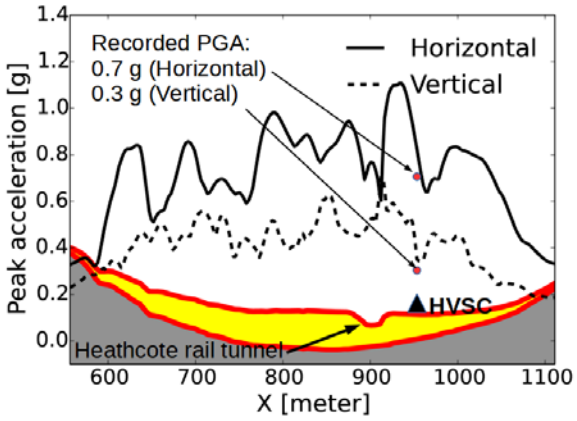

Figure 11. Simulated horizontal and vertical peak accelerations along the surface of the valley, subjected to the 04/09/2010 event. HVSC is located approximately 50 m away from an 8 m high steep slope. Both horizontal and vertical component show their peak accelerations behind the crest of this slope.

6 CONCLUSIONS

We presented a case study on the site amplification effects at Heathcote valley, observed during the 2010-2011 Canterbury earthquake sequence. A 3D representation of the geological structure of Heathcote Valley was developed using a LiDAR-based DEM and in-situ geophysical test data obtained by sCPT and MASW. Based on the 3D representation of the geological structure, a series of 2D dynamic finite element simulations were undertaken, assuming that deconvolved motions recorded at LPCC can be used as the input motions at the base of the numerical model. Comparisons of simulated and recorded motions demonstrated that the numerical model can accurately simulate the recorded response of the valley at HVSC, as long as the source is relatively far (i.e. the reference station assumption is valid); unfortunately for the near-field events, simulated and recorded motions showed poorer agreement.

Both the observation and the simulation showed strong amplification at f = 2-5 Hz in the horizontal component and f = 5-10 Hz in the vertical component. The simulations suggest that the strong impedance contrast at the soil-rock interface is likely the primary cause of the strong amplifications in the horizontal component. However, the comparison of the responses with and without the vertical input motion suggests that the vertical accelerations recorded at HVSC was strongly affected by the basin-induced Rayleigh waves, which dominates the vertical response over a broad range of frequencies. The spatial pattern of peak ground acceleration across the valley surface suggests that the ground motion intensities were likely the highest at the crest of a cut slope approximately 50 m away from HVSC, due to the additional amplification effects caused by the topographic irregularity.

7 ACKNOWLEDGEMENTS

Clinton M. Wood (University of Arkansas) kindly provided his MATLAB scripts for the beamforming analyses used in MASW surveys. Matthew Hughes (University of Canterbury) processed the DEM, which was used for modelling the surface topography. Financial support for this research was provided from the New Zealand Earthquake Commission (EQC) and Natural Hazards Research Platform.

8 REFERENCES

Ashford, S.A., Sitar, N., Lysmer, J. & Deng, N. 1997. Topographic effects on the seismic response of steep slopes, *Bull. Seismol. Soc. Am.*, 87: 701–709.

Assimaki, D. & Jeong, S. 2013. Ground-Motion Observations at Hotel Montana during the M 7.0 2010 Haiti Earthquake: Topography or Soil Amplification?, *Bull. Seismol. Soc. Am.*, 103: 2577–2590.

Beavan, J., Motagh, M., Fielding, E. J., Donnelly, N. & Collett, D. 2012. Fault slip models of the 2010-2011 Canterbury, New Zealand, earthquakes from geodetic data and observations of postseismic ground deformation. *New Zealand Journal of Geology and Geophysics,* 55(3): 207-221.

Bradley, B.A. 2012. Strong ground motion characteristics observed in the 4 September 2010 Darfield, New Zealand earthquake. *Soil Dynamics and Earthquake Engineering*, 42: 32-46.

Bradley, B.A. 2013. Systematic ground motion observations in the Canterbury earthquakes and region-specific non-ergodic empirical ground motion modeling, *Earthq. Spectra*, 131230112032001, doi:10.1193/053013EQS137M.

Bradley, B.A. & Cubrinovski, M. 2011. Near-source Strong Ground Motions Observed in the 22 February 2011 Christchurch Earthquake, *Seismol. Res. Lett.*, 82: 853–865, doi:10.1785/gssrl.82.6.853.

Brown, L.J., Reay, M.B. & Weeber, J.H. 1992. *Geology of the Christchurch urban area*, Institute of Geological and Nuclear Sciences.

Johnson, D.H. & Dudgeon, D.E. 1992. *Array signal processing: concepts and techniques*, Simon & Schuster.

Kawase, H. 1996. The cause of the damage belt in Kobe:"The basin-edge effect," constructive interference of the direct S-wave with the basin-induced diffracted/Rayleigh waves, *Seismol. Res. Lett.*, 67(5): 25–34.

Konno, K. & Ohmachi, T. 1998. Ground-motion characteristics estimated from spectral ratio between horizontal and vertical components of microtremor, *Bull. Seismol. Soc. Am.*, 88(1): 228–241.

Kuhlemeyer, R.L. & Lysmer, J. 1973. Finite element method accuracy for wave propagation problems, *J. Soil Mech. & Found. Div*, *99*(Tech Rpt).

Matheron, G. 1963. Principles of geostatistics, *Econ. Geol.*, 58(8): 1246–1266.

Mazzoni, S., McKenna, F., Scott, M.H. & Fenves, G.L. 2007. OpenSees Command Language Manual. Pacific Earthquake Engineering Research Center, *Univ. California, Berkeley*.

Park, C.B., Miller, R.D. & Xia, J. 1999. Multichannel analysis of surface waves, *Geophysics*, 64(3): 800–808, doi:10.1190/1.1444590.

Wathelet, M. 2005. GEOPSY Geophysical Signal Database for Noise Array Processing, *Software, LGIT, Grenoble, Fr.*

Wood, C.M., Cox, B.R., Wotherspoon, L.M. & Green, R.A. 2011. Dynamic site characterization of Christchurch strong motion stations, *Bull. New Zeal. Soc. Earthq. Eng.*, 44(4): 195–204.